SUPPLEMENTAL METHODS

Field deployment of ADCP moorings and OBSs

Eleven moorings with acoustic-Doppler current profilers (ADCPs) and twelve Ocean-Bottom Seismographs (OBSs) were deployed along the Submarine Congo Canyon-Channel between 9th September 2019 to 2nd October 2019, divided into canyon and channel sub-arrays (Fig. 1). The ADCPs were on a fixed mooring anchored within the canyon-channel, suspended 44-250 m above the canyon floor. In contrast, the OBS were deployed ~700-2900 m outside the canyon-channel, on flat canyon terraces or on overbank areas. The location of each OBS is based on the ship's position when the instrument was deployed, whilst the location of each ADCP mooring was confirmed to within +/- ~15 m by ultra-short baseline acoustic positioning. Three ADCP moorings surfaced in October 2019, while the remaining eight were broken by the powerful, >1,000 km runout 14-16th January 2020 turbidity current event, which also broke the SAT-3 (South Atlantic 3) and WACS (West Africa Cable System) cables. A second >1,000 km runout flow on 8th March 2020 broke the repaired SAT-3 cable. The OBSs were not damaged by the >1,000 km runout flows and recorded ~9-10 months of data, depending on battery life. Nine of eleven ADCP and ten of twelve OBS instruments were recovered. Figure 1 shows the locations of the ADCPs and OBSs used in the analysis.

OBS and ADCP instrument specifications

Eight of the nine recovered OBS stations consisted of three channel Sercel L28-LB geophones and a Hi-Tech HTI-90U hydrophone. The most distal seismic station (OBS9), located 1071 km offshore, contained a three channel Owen (4.5Hz) Geophone and a Hi-Tech HTI-04 hydrophone. The geophone data were analysed for turbidity current activity, which recorded the ground vibrations generated by passing turbidity current events, with all geophones having a sampling frequency of 1 kHz.

The downward pointing ADCPs deployed were a mixture of 75, 300, and 600 kHz ADCPs, which recorded a profile of water column velocity every 11 or 45 seconds, depending on the ADCP set-up (Talling et al., 2022; their Supplementary Table 2).

Identifying turbidity current events in ADCP and OBS data and calculating flow transit velocities

Turbidity currents were identified in the ADCP data by an abrupt increase in near-bed velocities above ambient values of ~0.3 m/s, and the start manually picked. The start of a turbidity current event at each OBS was manually picked from the exponential curve on vertical component of the seismic data, at the point that the signal increased above background due to a passing turbidity current.

The transit speed of the turbidity currents was calculated by dividing the distance between ADCP or OBS stations (measured along the sinuous canyon thalweg) with the difference in arrival times. The distance the flows travelled (runout distance) was defined as the location of the most distal station that a tracked flow signal was recorded at.

The timing of submarine telecommunication cables breaks were also used to define turbidity current arrival times and transit velocities. Here we assume that the time of the fault equals the time of the arrival of the turbidity current. Cable breaks were recorded to the nearest minute.

Time-lapse seafloor surveys and net eroded sediment volumes

Bathymetric data of the Congo Canyon and Channel was collected via swath multibeam surveys collected in September–October 2019 and October 2020 using a Kongsberg EM122 (1° x 1°) system operating at 12 kHz on the RRS James Cook (Fig. 1A). The beam swath width was set to the narrowest setting (45° from the nadir) to try and generate the highest resolution data possible.

The data were processed in CARIS HIPS and SIPS and corrected for the ship's motion and for differences in sound velocity in the water column (using data from a sound-velocity profiler). The data was gridded with horizontal grid cell dimension of 5 m (canyon survey) or 15 m (channel survey).

Erosion or deposition of sediment between the two surveys was determined by producing a bathymetric difference map in ArcGIS, where the September-October 2020 bathymetric data was subtracted from September–October 2019 bathymetric data (Fig. 1C, D). The bathymetric difference map shows the net change in seafloor elevation over the one-year period between the two bathymetry surveys. To derive the volume of net eroded sediment, the change in elevation for each grid cell within the canyon thalweg and channel floor were multiplied by grid cell areas. Volumes of net erosion did not include areas outside the canyon or channel.

The net eroded volume calculations assumes that measurement errors are symmetrically distributed about a zero value, and thus cancel out over the survey areas. This was confirmed with measurements of differences in seabed elevation on the bathymetric difference map for areas where it was assumed no significant change occurred for both the canyon and channel. For these areas, the mean difference in seabed elevation was generally found to be close to zero with the difference values equally distributed around the mean when plotted as a histogram (Talling et al. 2020; supplementary figures 7 and 8). This method thus returns a 'best guess' for volume of seabed change.

To calculate the organic carbon mass eroded along the length of canyon and channel, we used the total net eroded sediment volume (2.68 km^3) determined by Talling et al. (2022). For this calculation, Talling et al. (2022) used both the canyon and channel time-lapse surveys (Fig 1). These two surveys covered 40% (477 km of 1179 km) of entire length of the Congo Canyon-Channel, as measured along its sinuous axis. Talling et al. (2022) assumed similar rates of erosion in the intervening section of channel that was not surveyed, to calculate the total net eroded volume of sediment along the whole canyon-channel system.

Grain size and geochemical analysis of sediment samples

Grain-size analysis of the sediment samples was conducted on the Beckman Coulter LS 13 320 Laser Diffraction Particle Size Analyser at the Department of Geography, Durham University. 20 mL of 20% hydrogen peroxide was added to ~0.5 g of sediment sample to remove organics before the sample was centrifuged to remove the supernatant. Samples were then mixed with 20 mL of deionized water and 2 mL of sodium hexametaphosphate solution to limit

flocculation. Samples were run through the analyser three times; the runs were compared and if similar then the results were averaged.

The five core facies were identified as the sediment cores were visually logged based on visual characteristics and the feel of the material when rubbed between fingers. Clay bed facies were determined based on only smooth material felt between fingers, whilst silt contained a slight grittiness felt between fingers but with no grains visible using a hand-lens. The sand facies all had grains felt between fingers and visible with a hand lens, allowing the grain size to be determined. Muddy sand contained dark smooth mud in addition to the sand grains, whilst the sand facies was clean. Vegetation-rich muddy sand contained concentrated, well-preserved mm- to cm-sized black wood and plant debris, along with sand grains and a muddy matrix.

The carbon stable isotope composition ($\delta^{13}C$) of organic carbon (OC) is used to differentiate between marine and terrestrial organic matter, based on the assumption that marine organic matter is more depleted in ^{13}C compared to terrestrial organic matter (Burdige, 2005). Radiocarbon measurements were employed to determine the age of the OC and is expressed as 'fraction modern' (Fm). Fm is a measurement of the deviation of the $^{14}C/^{12}C$ ratio of a sample from "modern" (defined as 95% of the radiocarbon concentration in AD 1950). The Fm measurements are a bulk measurement of the sample, and thus the values can represent organic material of many ages and sources. Bulk OC Fm values can contain contributions from young terrestrial biospheric carbon produced by photosynthesis (Fm = ~1.0), old terrestrial biospheric carbon produced by degraded soil, and ancient (petrogenic) carbon from erosion of rocks which is ^{14}C free (Fm = 0) (Leithold et al., 2016; Hage et al., 2020). Future work could use additional techniques such as ramped pyrolysis–oxidation (RPO) to distinguish OC components.

Each sediment sample was measured for total organic carbon content (TOC), carbon stable isotope composition ($\delta^{13}C$) and radiocarbon content (expressed as 'fraction modern', Fm) at the Laboratory of Ion Beam Physics at ETH Zurich. About 60 mg of sediment was replaced in Ag capsules and treated with HCL 37% (65°C, 72 hours) to remove inorganic carbon. After neutralization with NaOH (65°C, 72 hours) samples were wrapped in tin boats. The TOC, radiocarbon and $\delta^{13}C$ composition of bulk OC were measured on an Elemental Analyzer-Isotope Ratio Mass Spectrometer (EA-IRMS, Elementar vario MICRO cube—Isoprime PresION) coupled to a Mini Carbon Dating System (MICADAS) Accelerator Mass Spectrometer. Based on peptone (Sigma) and atropine (Santis) standards, accuracy of TOC and $\delta^{13}C$, corresponded to values better than 0.03% and 0.1‰. Radiocarbon isotopic data were reduced using BATS software (Wacker et al., 2010) and reported radiocarbon data are expressed as F14 C (Fm) values (Reimer et al., 2004).

Published radiocarbon data from the Congo River from Hemingway et al. (2017), reported in Δ14C per-mille (‰) notation, was converted to Fm using:

$$F_m = \frac{\Delta 14C + 1000e^{-\frac{-(y-1950)}{8267}}}{1000}$$

Where *y* is the year of data collection (Torn et al., 2009). The radiocarbon data from the Congo Lobe in Savoye et al. (2009) were converted from radiocarbon years (conventional 14C age) to Fm using the following equation:

$$14C\ age = -8033Ln(F_m)$$

Organic carbon budget calculations

For the Congo Canyon organic carbon budget calculation, the total eroded sediment volume for the canyon floor (determined from the bathymetric difference map) needed to be converted to eroded dry sediment mass, via the sediment density (Tables S1 to S3). For this, the total eroded sediment volume was divided into the facies proportions averaged across the seven sediment cores (Table S1). This method assumes that the facies proportions, and associated facies sediment density within the cores, can be scaled up to represent the whole canyon floor. However, this is considered more precise than methods which assume blanket sediment density properties to convert from volume to mass.

To calculate the sediment density of each facies type, the porosity (ϕ) of the different facies was first derived from the gamma-ray wet density (ρ_w) values measured every 0.01 m from the Multi-Sensor Core Logger (GeoTek MSCL-S) via:

$$\phi = -\frac{(\rho_w - \rho_d)}{\rho_d - \rho_{sw}}$$

where ρ_{sw} is the density of seawater at 1.025 kg/m^3 and ρ_d is the sediment grain density of quartz at 2.6 kg/m^3. The average porosity for each facies in the sediment cores was averaged across six of the sediment cores and the standard deviation calculated, with core 1 discounted as the sediment had been remobilised (Table S2). The average facies porosity values ± standard deviation were converted into dry sediment density (ρ) using:

$$\rho = (1 - \phi) * \rho_d * 1000$$

From the dry sediment density, the facies mass eroded in Mt (Table S3) was calculated via:

$$M_f = (V * F) * \rho$$

where V is the total eroded volume in the canyon 0.32 km^3 and F is the facies proportion. The organic carbon mass eroded was then calculated using the average TOC (%) value ± standard deviation for each facies type (Table S3).

To calculate the organic carbon mass eroded along the length of canyon and channel, the total net eroded sediment volume along the whole canyon-channel determined by Talling et al. (2022) was used (2.68 km^3). First, the volume of sediment eroded from the canyon (0.32 km^3), for which the OC mass eroded was already well constrained, was subtracted from the total net eroded sediment volume. The remaining volume was converted to sediment and organic carbon mass using the estimated porosity and TOC values for the Congo Channel from Baudin et al. (2020). Baudin et al. (2020) suggest a porosity of 0.70% for sediment in the channel, to calculate the sediment mass we used a porosity range of 0.60% to 0.80%, based on global data for the upper 50 m of sediment (Kominz et al., 2011). A TOC value of 2.0 ± 0.1 % is used from Baudin et al. (2020) to convert from sediment to organic carbon mass.

REFERENCES

Baudin, F., Rabouille, C., and Dennielou, B., 2020, Routing of terrestrial organic matter from the Congo River to the ultimate sink in the abyss: a mass balance approach: Geologica Belgica, v. 23, p. 41–52, doi:10.20341/gb.2020.004.

Burdige, D.J., 2005, Burial of terrestrial organic matter in marine sediments: A re-

assessment: Global Biogeochemical Cycles, v. 19, p. 1–7, doi:10.1029/2004GB002368.

Hage, S. et al., 2020, Efficient preservation of young terrestrial organic carbon in sandy turbidity-current deposits: Geology, v. 48, p. 882–887, doi:10.1130/G47320.1.

Hemingway, J.D., Schefuß, E., Spencer, R.G.M., Dinga, B.J., Eglinton, T.I., McIntyre, C., and Galy, V. V., 2017, Hydrologic controls on seasonal and inter-annual variability of Congo River particulate organic matter source and reservoir age: Chemical Geology, v. 466, p. 454–465, doi:10.1016/j.chemgeo.2017.06.034.

Kominz, M.A., Patterson, K., and Odette, D., 2011, Lithology dependence of porosity in slope and deep marine sediments: Journal of Sedimentary Research, v. 81, p. 730–742, doi:10.2110/jsr.2011.60.

Leithold, E.L., Blair, N.E., and Wegmann, K.W., 2016, Source-to-sink sedimentary systems and global carbon burial: A river runs through it: Earth-Science Reviews, v. 153, p. 30–42, doi:10.1016/j.earscirev.2015.10.011.

Reimer, P.J., Brown, T.A., and Reimer, Ron, W., 2004, Discussion: Reporting and Calibration of Post-Bomb 14 C Data: Radiocarbon, v. 46, p. 1299–1304, doi:10.1017/S0033822200033154.

Savoye, B., Babonneau, N., Dennielou, B., and Bez, M., 2009, Geological overview of the Angola-Congo margin, the Congo deep-sea fan and its submarine valleys: Deep-Sea Research Part II: Topical Studies in Oceanography, v. 56, p. 2169–2182, doi:10.1016/j.dsr2.2009.04.001.

Talling, P.J. et al., 2022, Longest sediment flows yet measured show how major rivers connect efficiently to deep sea: Nature Communications, v. 13, p. 1–15, doi:10.1038/s41467-022-31689-3.

Torn, M.S., Swanston, C.W., Castanha, C., and Trumbore, S.E., 2009, Storage and Turnover of Organic Matter in Soil, *in* Biophysico-Chemical Processes Involving Natural Nonliving Organic Matter in Environmental Systems, Hoboken, NJ, USA, John Wiley & Sons, Inc., p. 219–272, doi:10.1002/9780470494950.ch6.

Wacker, L., Christl, M., and Synal, H.A., 2010, Bats: A new tool for AMS data reduction: Nuclear Instruments and Methods in Physics Research, Section B: Beam Interactions with Materials and Atoms, v. 268, p. 976–979, doi:10.1016/j.nimb.2009.10.078.

Fig S1. Timing and runout distance of turbidity current flows recorded by Ocean Bottom Seismometers (OBSs) and Acoustic Doppler Current Profilers in the Congo Canyon-Channel between October 2019 and April 2020.

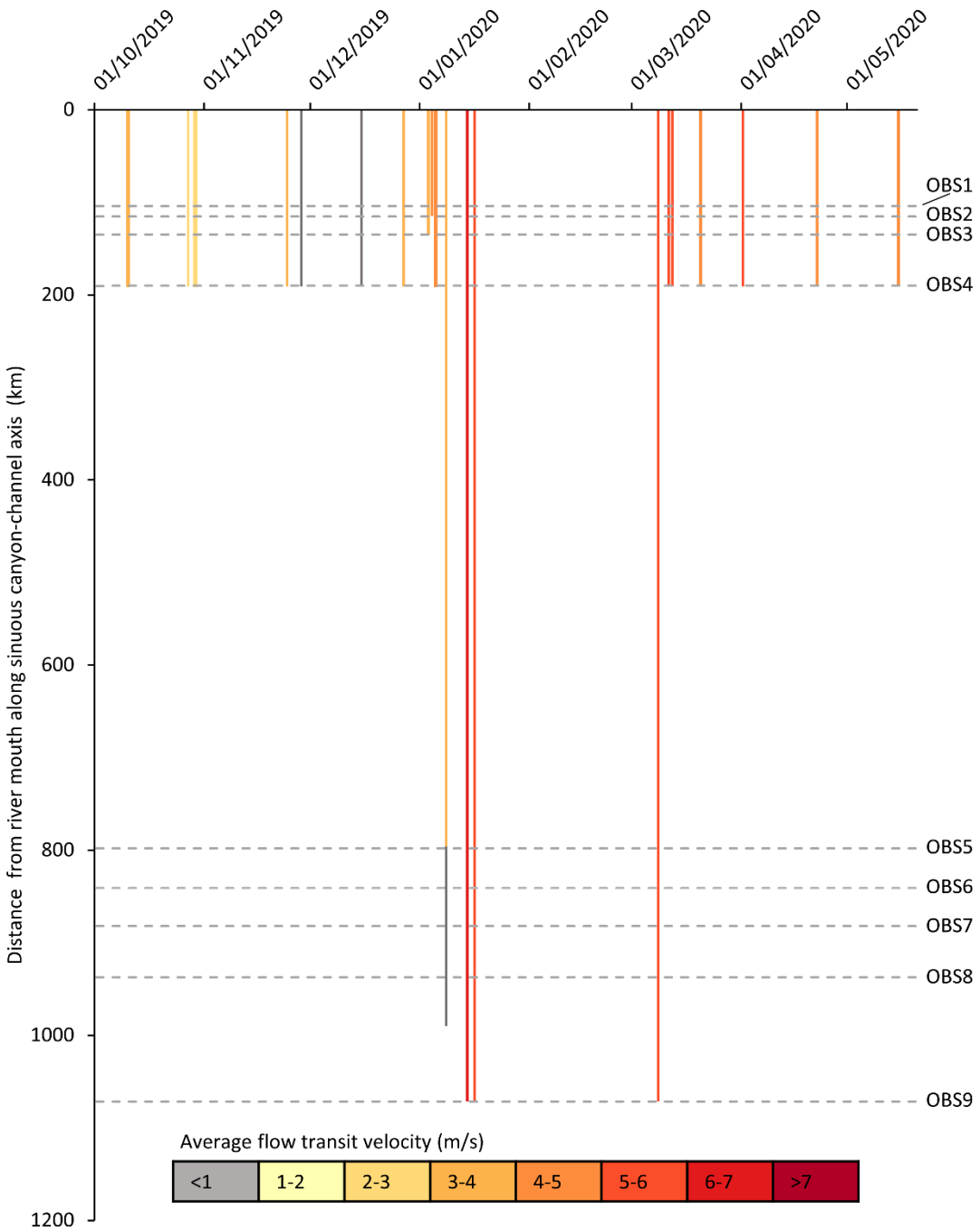

Supplementary Table 1. Length of each facies type in metres in each core

	Length of facies (m)				
Core	Clay	Silt	Muddy sand	Vegetation-rich muddy sand	Sand
1	0	0	0	0	1.50
2	1.37	0.05	1.24	0.00	0.10
3	0.50	0.51	1.04	1.06	1.03
4	5.03	0.60	0.42	0.03	1.38
5	3.45	0.65	1.45	0.33	0.57
6	1.38	4.77	2.71	0.10	0.19
7	5.92	1.74	0.06	0.00	0.00
Total length (m)	**6.93**	**17.65**	**3.28**	**8.33**	**1.52**
Proportion (%)	18.38	46.81	8.69	22.09	4.04

Note: Core 1 was discounted from the calculations as sediment recovery was compromised by bent barrel.

Supplementary Table 2. Average porosity values of the different facies in the Congo Canyon sediment cores

Core	Average porosity per facies per core (%)				
	Clay	Silt	Muddy sand	Vegetation-rich muddy sand	Sand
2	0.80	0.74	0.69		0.64
3	0.76	0.77	0.70	0.80	0.58
4	0.74	0.75	0.64	0.73	0.46
5	0.74	0.65	0.62	0.78	0.68
6	0.77	0.72	0.60	0.71	0.49
7	0.82	0.79	0.78	/	/
Average Porosity (%)	**0.77**	**0.74**	**0.67**	**0.76**	**0.57**
Porosity standard deviation (%)	0.03	0.04	0.06	0.04	0.08

Note: Core 1 was discounted as the sediment had been remobilised.

Supplementary Table 3. Values Needed to Calculate Mass of Sediment and Organic Carbon Eroded in the Congo Canyon Between October 2019 and October 2020

	Facies				
	Clay	Silt	Muddy sand	Vegetation-rich muddy sand	Sand
Facies proportion (%; Table S1)	18.38	46.81	8.69	22.09	4.04
Average facies porosity (%, Table S2)	0.77	0.74	0.67	0.76	0.57
Standard deviation of facies porosity (%, Table S2)	0.03	0.04	0.06	0.04	0.08
Facies density (kg/m^3)	598	676	858	624	1118
Facies density error (kg/m^3)	77	116	156	95	219
Sediment eroded (Mt)	**89**	**48**	**50**	**8**	**31**
Sediment eroded error (Mt)	**12**	**8**	**9**	**1**	**6**
Average facies TOC (%, Table S4)	3.51	2.60	1.81	8.24	0.49
Standard deviation facies TOC (%)	0.60	0.99	1.74	2.24	0.26
Average facies δ13C (‰,Table S4)	-26.72	-26.97	-27.21	-27.32	-27.36
Average facies Fm (Table S4)	0.9446	0.9526	0.9121	0.9881	0.7784
TOC eroded (Mt)	**3.13**	**1.24**	**0.91**	**0.66**	**0.15**
TOC eroded error (Mt)	**0.87**	**0.60**	**0.88**	**0.25**	**0.09**

Supplementary Table 4: Facies Description and Geochemical Data

	Facies description	Average Total Organic Carbon (TOC) and [range] (%)	Average Carbon-Stable Isotope (δ13C) and [range] (‰)	Average Fraction Modern (Fm) and [range]
Clay	Homogeneous or bioturbated clay. Black organic matter particles visible.	**3.51** [5.46 — 2.39]	**-26.72** [-27.30 — -26.29, anomalous value = -23.83]	**0.9446** [0.8484 — 0.9945]
Silt	Homogeneous or bioturbated silty mud. Occasional normal grading to clay or laminated. Often high number of black organic carbon specks.	**2.60** [5.22 — 1.61]	**-26.97** [-27.71—-26.63]	**0.9526** [0.9152 — 0.9814]
Muddy sand	Mixed sand-mud with fine- to medium-grained sand. Occasional floating mud, sand or vegetation-rich muddy sand clasts. Ungraded or normally graded. Organic specks often visible.	**1.81** [0.25 — 6.23]	**-27.21** [-28.45 — -26.38]	**0.9121** [0.8051 — 1.0448]
Vegetation-rich muddy sand	Muddy-sand matrix (fine-grained sand) dominated by mm- to cm-sized black plant debris which can be densely packed.	**8.24** [4.57— 11.32]	**-27.32** [-27.80 — -22.16, anomalous value = -22.16]	**0.9881** [0.9528 — 1.0184, anomalous value = 0.7037]
Sand	Massive, clean fine- to medium-grained sand. occasional floating mud and muddy sand clasts. Often ungraded, occasionally normally graded.	**0.49** [0.15 — 0.88]	**-27.36** [-28.19 — -26.96]	**0.7784** [0.6758 —0.8639]

Supplementary Table 5. Organic carbon geochemistry and grain size on all samples for this study.

ETH number	Sample code	Core depth (m)	Facies	$F^{14}C$ (mean)	$F^{14}C$ uncertainty (%)	Age (y)	Age uncertainty (y)	D_{10} (µm)	D_{50} (µm)	D_{90} (µm)	δ13C (‰)	TOC (%)
	PC04-1-6	0.06	Clay					0.7	5.6	30.4	-26.64	2.98
	PC04-1-90	0.90	Clay					0.7	5.8	29.8	-26.73	2.66
120320.1.1	PC04-2-2	1.21	Silt	0.9699	0.82	245	66	1.2	20.1	98.4		
120321.1.1	PC04-2-23	1.42	Silt	0.9814	0.86	151	69	1.8	48.9	111.9		
120322.1.1	PC04-2-85	2.04	Clay	0.9401	0.82	496	66	1.0	14.2	73.7	-26.58	3.34
120338.1.1	PC04-3-35	3.01	Clay	0.9257	0.86	620	69	0.9	11.4	77.7	-26.59	4.03
120339.1.1	PC04-4-70	4.00	Clay	0.9945	0.84	44	68	1.1	13.9	69.5	-26.39	3.99
120340.1.1	PC04-4-90	4.20	Clay	0.9594	0.86	333	69	1.2	11.8	65.2	-26.33	5.46
120341.1.1	PC04-5-15	5.97	Clay	0.9533	0.85	384	68	0.8	7.9	49.3		3.79
120342.1.1	PC04-5-115	4.97	Clay	0.9520	0.84	395	67	0.9	10.6	55.2		3.93
120343.1.1	PC04-6-60	7.59	Clay	0.9770	0.84	187	68	1.1	11.1	46.9		
120344.1.1	PC04-6-130	6.89	Clay	0.9161	0.85	704	68	1.1	13.5	61.7		
120927.1.1	PC07-1-10	0.10	Sand	0.7377	0.95	2,443	77	72.0	129.6	211.9		
	PC07-1-50	0.50	MS					3.3	168.6	500.3	-27.50	0.63
120986.1.1	PC07-1-95	0.95	MS	0.8455	0.89	1,348	71	7.1	127.9	375.8	-27.42	0.82
120990.1.1	PC07-2-5	1.51	Clay	0.9631	0.84	302	68	0.8	6.0	29.4	-27.30	3.92
120984.1.1	PC07-2-55	2.01	Silt	0.9478	0.85	431	68	1.5	45.7	187.0	-27.12	2.61
120991.1.1	PC07-3-35	2.39	Silt	0.9806	0.85	158	69	1.2	34.4	148.1	-27.32	2.14
120931.1.1	PC07-3-90	2.94	MS	0.9562	0.81	360	65	3.1	86.5	187.9		2.39
120939.1.1	PC07-3-110	3.14	VRMS	0.9973	0.81	22	65	9.5	100.4	190.2	-27.52	7.90
120930.1.1	PC07-3-136	3.40	MS	1.0448	0.81	0	65	5.0	102.9	231.5	-26.38	6.23
120935.1.1	PC07-4-60	4.11	Clay	0.9346	0.80	543	65	0.8	7.7	37.3		
120992.1.1	PC07-4-110	4.61	MS	0.9429	0.85	472	68	2.5	79.2	290.3	-27.21	1.93
120988.1.1	PC07-5-5	5.03	Clay	0.9537	0.86	381	69	0.9	11.3	77.8	-27.00	3.19
120938.1.1	PC07-5-70	5.68	MS	0.8051	0.88	1,741	71	50.7	205.6	452.7	-28.45	0.25

120940.1.1	PC07-5-122	6.20	Clay	0.9436	0.80	466	64	0.9	6.2	26.9	-27.13	3.65
120285.1.1	PC08-1-1	0.01	VRMS	0.9721	0.83	227	67	5.4	89.1	187.6	-26.98	6.46
120286.1.1	PC08-1-90	0.90	Clay	0.9932	0.84	55	67	1.1	8.3	45.1	-26.67	3.68
120287.1.1	PC08-2-25	1.72	Clay	0.9499	0.85	413	68	0.9	9.7	58.1	-27.07	2.39
120288.1.1	PC08-2-110	2.57	Silt	0.9721	0.84	227	67	1.2	20.6	91.4	-26.78	2.27
120289.1.1	PC08-3-8	2.98	Clay	0.9605	0.84	324	68	0.9	10.9	65.3		3.35
120290.1.1	PC08-3-11	3.01	Sand	0.7509	0.99	2,301	79	36.7	122.6	224.7	-26.91	
120291.1.1	PC08-3-70	3.60	Clay	0.9607	0.82	322	66	1.0	6.6	29.3	-26.59	3.49
120292.1.1	PC08-4-31	3.92	Silt	0.9152	0.86	712	69	1.4	37.3	283.2	-26.74	1.75
120293.1.1	PC08-4-80	4.41	Clay	0.9720	0.84	229	68	0.9	8.2	49.0	-26.76	3.93
120294.1.1	PC08-4-130	4.91	Clay	0.9429	0.84	472	67	0.9	6.7	29.9	-26.85	3.25
120295.1.1	PC08-5-34	5.42	MS	0.8394	0.88	1,406	71	3.0	88.4	206.7	-26.88	1.08
120296.1.1	PC08-5-85	5.93	Sand					91.4	188.4	322.4	-27.19	
120297.1.1	PC08-5-135	6.43	Sand	0.6758	0.98	3,148	79	106.1	279.6	505.9	-27.30	
120298.1.1	PC08-6-50	6.99	Sand	0.7811	0.93	1,985	75	95.0	231.5	465.8	-27.31	0.15
120299.1.1	PC08-6-100	7.49	Clay	0.8737	0.84	1,085	67	0.9	9.0	59.3	-26.52	2.66
120284.1.1	PC08-6-142	7.91	MS	0.8863	0.85	970	68	4.0	127.8	308.5	-26.91	1.20
120936.1.1	PC12-1-12	0.12	Sand	0.7525	1.07	2,284	86	83.3	196.2	411.5		
120934.1.1	PC12-1-25	0.25	Silt	0.9770	0.81	187	65	1.9	51.3	184.4		
	PC12_1_50	0.50	MS					3.8	87.6	212.8	-27.37	1.48
120932.1.1	PC12-1-70	0.70	MS	0.9857	0.84	116	68	4.7	86.6	332.9	-26.90	6.22
120933.1.1	PC12-1-100	1.00	VRMS	0.9528	0.83	389	67	5.9	86.9	256.0	-27.80	9.95
120989.1.1	PC12-2-40	1.60	Sand	0.8639	0.87	1,176	70	2.5	86.8	203.0	-27.30	0.88
120987.1.1	PC12-2-85	2.05	VRMS	0.9999	0.84	0	68	6.7	90.3	231.2	-27.25	11.32
120985.1.1	PC12-2-130	2.50	Clay	0.8484	0.89	1,320	72				-26.36	3.03
120929.1.1	PC12-3-15	2.82	MS	0.9606	1.10	323	88	2.0	68.2	179.7	-27.45	4.14
120928.1.1	PC12-3-37	3.04	Sand	0.8155	0.88	1,639	70	12.6	127.9	308.5	-26.96	0.49
120937.1.1	PC12-3-50	3.17	Clay	0.8578	0.82	1,232	66	1.1	7.7	37.7	-26.29	3.87
	PC12_3_66	3.33	Sand					68.6	176.9	354.2	-28.01	0.27
	PC12_3_110	3.77	Sand					79.4	202.7	426.7	-27.11	

120345.1.1	PC14-1-2	0.02	Silt	0.9444	0.88	460	70	5.5	60.8	119.3	-27.12	1.61
	PC14-1-50	0.50	Clay					0.7	5.0	19.2	-27.19	3.28
	PC14-1-95	0.95	MS					49.7	105.8	153.3	-27.65	0.38
120925.1.1	PC14-2-11	1.39	Silt	0.9270	0.85	609	68	1.4	23.4	241.6	-27.71	3.36
120926.1.1	PC14-2-14	1.42	Sand	0.8497	0.85	1,309	68	7.1	105.8	281.5	-28.19	0.65
120924.1.1	PC14-2-65	1.93	MS	0.8834	0.84	996	68	4.6	64.8	120.7	-26.86	0.96
	PC14-2-120	2.48	Silt					1.9	39.1	130.0	-26.63	5.22
120316.1.1	PC16-1-10	0.10	Sand					94.8	156.4	232.5		
120317.1.1	PC16-1-135	1.35	Sand					114.0	230.8	413.8		
120300.1.1	PC17-1-2	0.02	Clay	0.9455	0.82	450	66	1.2	8.2	41.2	-23.83	3.32
120301.1.1	PC17-1-50	0.50	MS	0.9358	0.84	533	68	2.9	84.8	181.6	-27.19	1.50
120302.1.1	PC17-2-59	1.10	MS	0.9080	0.84	776	68	2.0	71.2	342.1		1.14
120303.1.1	PC17-2-100	1.51	MS	0.9374	0.84	519	67	2.8	101.1	336.2	-27.15	1.43
120304.1.1	PC17-2-140	1.91	MS	0.9450	0.84	454	67	1.9	76.0	275.7		
120305.1.1	PC17-3-45	2.45	Silt	0.9470	0.84	438	67	1.3	26.6	157.7	-26.65	2.56
120306.1.1	PC17-3-87	2.87	Silt	0.9431	0.84	471	68	1.5	42.9	262.5	-26.95	2.20
120307.1.1	PC17-4-50	4.01	MS	0.8484	0.88	1,321	71	6.3	97.5	202.8	-26.94	0.49
120308.1.1	PC17-4-120	4.71	Silt	0.9155	0.84	709	68	1.6	27.0	127.4	-26.71	2.31
120309.1.1	PC17-5-55	5.36	MS	0.9192	0.85	677	68	3.9	67.9	139.6	-27.27	1.44
120310.1.1	PC17-5-58	5.39	Clay	0.9731	0.82	219	66	0.8	8.5	54.1	-26.76	3.10
120311.1.1	PC17-6-50	6.73	MS	0.8692	0.88	1,126	70	6.4	136.4	380.4	-27.16	0.61
120312.1.1	PC17-6-130	7.53	Clay	0.9668	0.83	271	67	0.9	8.8	39.6	-26.64	3.91
120313.1.1	PC17-7-70	8.43	Clay	0.9751	0.85	203	68	0.9	8.0	42.1	-26.81	3.47
120314.1.1	PC17-7-128	9.01	VRMS	1.0184	0.84	0	68	53.9	108.1	164.6	-22.16	4.57
120315.1.1	PC17-7-135	9.08	VRMS	0.7037	0.97	2,822	78	41.2	149.6	278.8	-27.03	9.26

Note: For facies, VRMS = vegetation-rich muddy sand, MS = muddy sand